to have survived for most of the lifetime of the cluster in its original orbit suggests that dynamical disruption in clusters is not sufficient to completely destroy any planetary population. It appears then that the lack of close-in planets may reflect a metallicity dependence in the migration mechanism or is evidence for the crowding in young clusters to suppress migration but not formation.

References and Notes
1. H. B. Richer *et al.*, *Astrophys. J.* **484**, 741 (1997).
2. B. Hansen *et al.*, *Astrophys. J.* **574**, L155 (2002).
3. A. G. Lyne *et al.*, *Nature* **332**, 45 (1987).
4. J. McKenna, A. G. Lyne, *Nature* **336**, 47 (1988).
5. S. E. Thorsett, Z. Arzoumanian, F. Camilo, A. G. Lyne, *Astrophys. J.* **523**, 763 (1999).
6. Thorsett *et al.*, in preparation, have an analysis of additional pulsar timing data consistent with the scenario discussed here.
7. D. Backer, R. S. Foster, S. Sallmen, *Nature* **365**, 817 (1993).
8. S. E. Thorsett, Z. Arzoumanian, J. H. Taylor, *Astrophys. J.* **412**, L33 (1993).
9. S. Sigurdsson, *Astrophys. J.* **415**, L43 (1993).
10. S. Sigurdsson, *Astrophys. J.* **452**, 323 (1995).
11. F. C. Michel, *Astrophys. J.* **432**, 239 (1994).
12. F. A. Rasio, *Astrophys. J.* **427**, L107 (1994).
13. E. B. Ford, K. J. Joshi, F. A. Rasio, B. Zbarsky, *Astrophys. J.* **528**, 336 (2000).
14. The Kozai mechanism works for stable triple systems in non-coplanar orbits and allows a trade-off between the relative inclination and the eccentricity of the system while preserving the product $(1 - e^2)\cos^2 i$. The proposed model can generate the observed eccentricity on time scales of 10^8 years.
15. S. Sigurdsson, *Astrophys. J.* **399**, L95 (1992).
16. K. J. Joshi, F. A. Rasio, *Astrophys. J.* **479**, 948 (1997).
17. H. B. Richer *et al.*, *Astrophys. J.* **574**, L151 (2002).
18. Measuring absolute position is more uncertain than measuring relative positions because of a lack of astrometric reference stars on the images. Our confidence in the absolute positions of well-measured stars is limited by the accuracy of the locations of the HST-catalogued guide stars which is $\pm 0.7''$. The pulsar position is relative to the HST guide stars used for these observations.
19. I. R. King, J. Anderson, A. M. Cool, G. Piotto, *Astrophys. J.* **492**, L37 (1998).
20. C. D. Bailyn *et al.*, *Astrophys. J.* **433**, L89 (1994).
21. A. Shearer, R. Butler, R. M. Redfern, M. Cullum, A. C. Danks, *Astrophys. J.* **473**, L115 (1996).
22. The region imaged near the pulsar location has an area of 1.75 square arcminutes. It contains 430 detected stars, so the prior probability of a random star in the pulsar error circle is 11%. Twenty-six stars in this region are white dwarfs, spread almost uniformly in area, and the majority are fainter than our candidate pulsar companion. The formal prior probability of finding a random superposed white dwarf there is 0.6%. At $V = 24.0$, the detection incompleteness is negligible; the white dwarf is far above the faintness limit of these images. Furthermore, the white dwarf lies above the normal cooling sequence, as befitting its undermassive status. Only 3 of the 26 white dwarfs in this field have this property. The probability of this occurring is thus only 0.07%. Figure 2 shows data from all the available fields, including more objects from a much wider area in order to define the white-dwarf cooling sequence more robustly.
23. R. Kippenhahn, A. Weigert, *Z. Astrophys.* **65**, 251 (1967).
24. When an evolved star in a close binary expands to become a giant, its outer envelope is stripped by the companion, leading to a truncation of the stellar evolution. This results in a white dwarf of lower mass than one that results from single-star evolution. The core never gets large enough to burn helium to carbon, and the white dwarf is composed of helium rather than the typical carbon and oxygen.
25. B. Hansen, E. S. Phinney, *Mon. Not. R. Astron. Soc.* **294**, 557 (1998).
26. Nuclear burning in thick hydrogen surface layers can slow the cooling for very low mass white dwarfs, but the effect is small for white dwarfs of mass $M > 0.25$ $M_\odot$. This has been established on both observational (*36*) and theoretical grounds (*37*).
27. In order for the postexchange orbit to be 0.3 AU, the preexchange orbit must have been about 0.2 AU. The preexchange companion of the neutron star likely was less massive than the current turn-off mass. It is possible, but unlikely, to form a neutron star in a binary with a low-mass main-sequence star at such an orbital semimajor axis. Such a system would not have a low enough space velocity to remain bound to the cluster after formation. Neutron star–white dwarf binaries descended from intermediate mass systems may form with high probability with the right semimajor axis and low space velocities.
28. F. Camilo, D. J. Nice, J. A. Shrauner, J. H. Taylor, *Astrophys. J.* **469**, 819 (1996).
29. R. Gilliland *et al.*, *Astrophys. J.* **545**, L47 (2000).
30. N. C. Santos, G. Israelian, M. Mayor, *Astron. Astrophys.* **373**, 1019 (2001).
31. D. N. C. Lin, P. Bodenheimer, D. C. Richardson, *Nature* **380**, 606 (1996).
32. N. Murray, D. Hansen, M. Holman, S. Tremaine, *Science* **279**, 69 (1998).
33. M. B. Davies, S. Sigurdsson, *Mon. Not. R. Astron. Soc.* **324**, 612 (2001).
34. I. A. Bonnell, K. W. Smith, M. B. Davies, K. Horne, *Mon. Not. R. Astron. Soc.* **322**, 859 (2001).
35. M4 currently has substantially lower stellar density in the core than 47 Tucanae, which may be a factor in the current absence of observed planets in 47 Tucanae.
36. M. H. van Kerkwijk, J. F. Bell, V. M. Kaspi, S. R. Kulkarni, *Astrophys. J.* **530**, L37 (2000).
37. B. M. S. Hansen, V. Kalogera, F. A. Rasio, *Astrophys. J.* **586**, 1364 (2003).
38. W. E. Harris, *Astron. J.*, **112**, 1487 (1996).
39. J. S. Kalirai *et al.*, in preparation; preprint available online at http://arxiv.org/abs/astro-ph/?0304036.
40. We would like to thank C. Bailyn and F. Rasio for useful discussions. The authors acknowledge the hospitality of the Kavli Institute for Theoretical Physics, supported by NSF grant PHY99-07949. S.S. is supported by NSF grant PHY-0203046, the Center for Gravitational Wave Physics, and the Pennsylvania State University Astrobiology Research Center. The Center for Gravitational Wave Physics is supported by the NSF under cooperative agreement PHY 01-14375. H.B.R. and I.H.S. are supported in part by grants from the Natural Sciences and Engineering Research Council (NSERC) of Canada. H.B.R. is also supported by the Canada Council through a Killam Fellowship. I.H.S. holds an NSERC University Faculty Award. B.M.H. is supported by HST grant HST-GO-08679.10A, provided by NASA through a grant from the Space Telescope Science Institute, which is operated by the Association of Universities for Research in Astronomy, Incorporated, under NASA contract NAS5-26555. S.E.T. is supported by NSF grant AST-0098343.

Atomic Memory for Correlated Photon States

C. H. van der Wal,[1] M. D. Eisaman,[1] A. André,[1] R. L. Walsworth,[2] D. F. Phillips,[2] A. S. Zibrov,[1,2,3] M. D. Lukin[1]*

We experimentally demonstrate emission of two quantum-mechanically correlated light pulses with a time delay that is coherently controlled via temporal storage of photonic states in an ensemble of rubidium atoms. The experiment is based on Raman scattering, which produces correlated pairs of spin-flipped atoms and photons, followed by coherent conversion of the atomic states into a different photon beam after a controllable delay. This resonant nonlinear optical process is a promising technique for potential applications in quantum communication.

The realization of many basic concepts in quantum information science requires the use of photons as quantum information carriers and matter (e.g., spins) as quantum memory elements (*1*). For example, intermediate memory nodes are essential for quantum communication and quantum cryptography over long photonic channels (*2*). Thus, methods to facilitate quantum state exchange between light and matter are now being actively explored (*3–5*). We report a proof-of-principle demonstration of a technique in which two correlated light pulses can be generated with a time delay that is coherently controlled via the storage of quantum photonic states in an ensemble of Rb atoms. This resonant nonlinear optical technique is an important element of a promising approach to long-distance quantum communication, proposed recently by Duan *et al.* (*6*). This proposal is based on earlier theoretical suggestions (*7, 8*) for storing photonic states in atomic ensembles [for a recent review see, e.g. (*9*)].

Our approach involves coherent control of the optical properties of an atomic ensemble and is closely related to studies involving electromagnetically induced transparency (EIT) (*10–12*) and resonantly enhanced nonlinear optical processes (*13, 14*) in a highly dispersive medium (*15, 16*). The use of such processes for nonclassical light generation has been extensively studied theoretically (*17–21*) and is probed experimentally in the present work. Storage of weak classical light pulses has been demonstrated (*22–24*); also, nonclassical spin

---
[1]Department of Physics, Harvard University, Cambridge, MA 02138, USA. [2]Harvard-Smithsonian Center for Astrophysics, Cambridge, MA 02138, USA. [3]P. N. Lebedev Institute of Physics, Moscow 117924, Russia.

*To whom correspondence should be addressed. E-mail: lukin@physics.harvard.edu
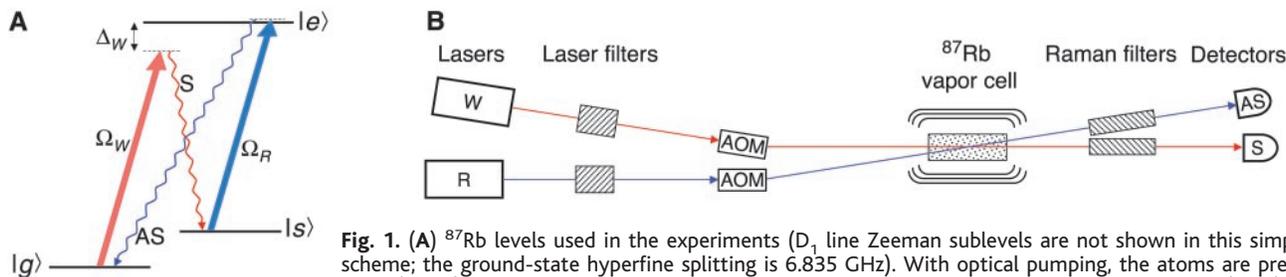
Fig. 1. (**A**) ^{87}Rb levels used in the experiments (D$_1$ line Zeeman sublevels are not shown in this simplified scheme; the ground-state hyperfine splitting is 6.835 GHz). With optical pumping, the atoms are prepared in the $|g\rangle = |5^2S_{1/2}, F = 1\rangle$ state. The write step (red) is a spontaneous Raman transition into the $|s\rangle = |5^2S_{1/2}, F = 2\rangle$ state. The transition is induced with a control beam with Rabi frequency Ω_W that couples $|g\rangle$ with detuning Δ_W to the excited state $|e\rangle$ (two nearly degenerate hyperfine levels $|5^2P_{1/2}, F' = 1\rangle$ and $|5^2P_{1/2}, F' = 2\rangle$). This Raman process creates a Stokes signal field (S) and a small population in the $|s\rangle$ state with a corresponding $|g\rangle\langle s|$ coherence. In the retrieve step (blue), this coherence is mapped back into an anti-Stokes field (AS) via a second Raman transition induced with a near-resonant retrieve control beam with Rabi frequency Ω_R. (**B**) Schematic of the experimental setup. Two lasers provide the write (W) and retrieve (R) control beams, with acousto-optic pulse modulation (AOM). The volumes of the two control beams overlap in the Rb vapor cell. The Stokes and anti-Stokes signal fields copropagate with the write and retrieve control beams, respectively, and a small angle between the control beams allows for spatially separated detection of the Stokes and anti-Stokes signals. The vapor cell is placed in an oven inside three layers of magnetic shielding. Filters after the lasers are used to suppress the spontaneous emission background and spurious modes of the lasers. Filters before the detectors block the transmitted control beams such that only the Stokes and anti-Stokes fields are detected.

states have been prepared in atomic ensembles (*25, 26*) and entanglement of two macroscopic ensembles has been observed (*27*).

Our experiment can be understood qualitatively by considering a three-state "lambda" configuration of atomic states coupled by a pair of optical control fields (Fig. 1A). A large ensemble of atoms is initially prepared in the ground state $|g\rangle$. Atomic spin excitations are produced via spontaneous Raman scattering (*28*), induced by an off-resonant control beam with Rabi frequency Ω_W and detuning Δ_W, which we refer to as the write beam. In this process, correlated pairs of frequency-shifted photons (so-called Stokes photons) and flipped atomic spins are created (corresponding to atomic Raman transitions into the state $|s\rangle$). Energy and momentum conservation ensure that for each Stokes photon emitted in a particular direction, there exists exactly one flipped spin quantum in a well-defined spin-wave mode. As a result, the number of spin-wave quanta and the number of photons in the Stokes field are strongly correlated. These atom-photon correlations closely resemble those between two electromagnetic field modes in parametric down-conversion (*29, 30*).

The state stored in the spin wave can be retrieved with a second Raman transition: A coherent conversion of the spin state into a different light beam (referred to as the anti-Stokes field) is accomplished by applying a second control beam (the retrieve beam) with Rabi frequency Ω_R (Fig. 1A). This Raman transition is not spontaneous; rather, it results from the atomic spin coherence interacting with the retrieve beam to generate the anti-Stokes field. The physical mechanism for this process is identical to the retrieval of weak classical input pulses (*31*) discussed in the context of "light storage" experiments (*22, 23*). As a result of the suppression of resonant absorption associated with EIT, the retrieved anti-Stokes field is not reabsorbed by the optically
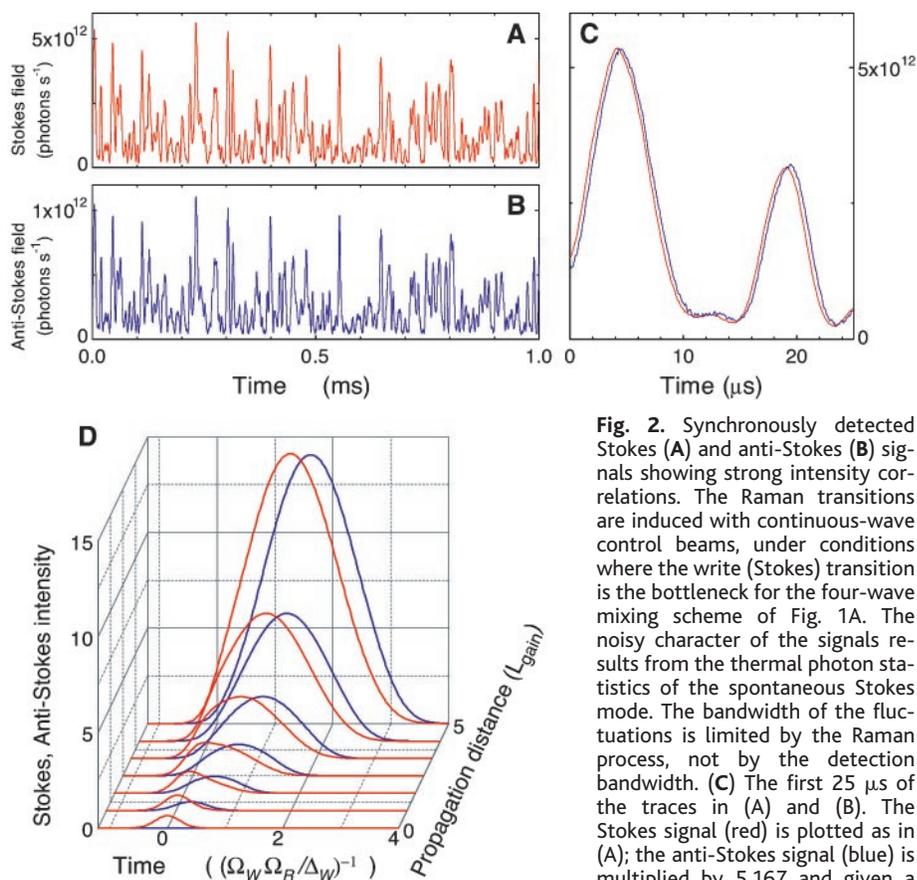
Fig. 2. Synchronously detected Stokes (**A**) and anti-Stokes (**B**) signals showing strong intensity correlations. The Raman transitions are induced with continuous-wave control beams, under conditions where the write (Stokes) transition is the bottleneck for the four-wave mixing scheme of Fig. 1A. The noisy character of the signals results from the thermal photon statistics of the spontaneous Stokes mode. The bandwidth of the fluctuations is limited by the Raman process, not by the detection bandwidth. (**C**) The first 25 μs of the traces in (A) and (B). The Stokes signal (red) is plotted as in (A); the anti-Stokes signal (blue) is multiplied by 5.167 and given a small intensity offset (to correct for a weak constant background signal from the control beam leaking through the filter) to match the Stokes signal. The anti-Stokes signal is delayed with respect to the Stokes signal (here measured to be 292 ns) as a result of the finite time the atoms spend in state $|s\rangle$ before conversion of the spin coherence into an anti-Stokes field. (**D**) Theoretically simulated propagation dynamics of Stokes (red) and corresponding anti-Stokes (blue) intensities in the continuous-wave excitation regime. An initial Stokes fluctuation propagates and evolves into an amplified pair of Stokes and anti-Stokes light pulses with locked propagation. The delay between the two Raman fields originates from the time it takes to convert the $|g\rangle\langle s|$ spin coherence into an anti-Stokes light pulse. This semiclassical simulation represents the solution of a boundary-value problem and is based on equations 38 to 41, 48, and 49 of (*14*), in which the effects of group velocities are included. The intensities are normalized to the amplitude of the initial Stokes fluctuation. The simulations assume nondecaying spin coherence, resulting in 100% retrieval efficiency. The propagation distance is in units of the four-wave mixing gain length $L_{gain} = v_g(\Omega_W\Omega_R/\Delta_W)^{-1}$, and time is in units of the inverse Raman bandwidth $(\Omega_W\Omega_R/\Delta_W)^{-1}$; see (*14*) and Fig. 1A.

dense cloud of atoms. Hence, this retrieval process allows, in principle, for an ideal mapping of the quantum state of a spin wave onto a propagating anti-Stokes field, which is delayed but otherwise identical to the Stokes field in terms of photon number correlations. The variable delay (storage time) and the rate of retrieval are controlled by the timing and the intensity of the retrieve beam.

In our experiment, we explore correlations between the photon fields associated with the preparation and retrieval of the atomic spin state. The onset of quantum-mechanical correlations between the photon numbers of the Stokes and delayed anti-Stokes light [analogous to twin-mode photon number squeezing (32, 33)] provides evidence for the storage and retrieval of nonclassical states. A schematic of the experimental apparatus is shown in Fig. 1B. An ^{87}Rb vapor cell with external antireflection-coated windows and a length of 4 cm is maintained at a temperature of typically ~85°C, corresponding to an atom number density of ~10^{12} cm^{-3}. Long-lived hyperfine sublevels of the electronic ground state are used as the storage states $|g\rangle$ and $|s\rangle$ (34).

We first present the results of simultaneous, continuous-wave (cw) excitation by both the write and retrieve control beams. Figure 2 presents an example of synchronously detected signals at the Stokes and anti-Stokes frequencies (Fig. 1A) in modes that copropagate with the control beams. The observed Stokes light (Fig. 2A) is a sequence of spontaneous pulses, each containing a macroscopic number of photons but with substantially fluctuating intensities and durations. The pulses were observed to have 10^3 to 10^7 photons, with an average depending on the write beam intensity and detuning and the atomic density. We estimate that the Raman gain coefficient could be varied over a broad range from ~e^1 to e^{20} by relatively small changes of these parameters (14).

The observed fluctuations are due to the spontaneous nature of the Raman scattering process, which corresponds to super-Poissonian photon number statistics (see also Fig. 3C). The observation of such photon statistics indicates that the transverse mode structure of the Raman fields is approximated reasonably well by a single spatial mode (28). In essence, each pulse corresponds to a spontaneously emitted Stokes photon that subsequently stimulates the emission of a number of other photons. As each Stokes photon emission results in an atomic transition from the state $|g\rangle$ into the spin-flipped state $|s\rangle$, the Stokes light fluctuations are mirrored in the anti-Stokes light (Fig. 2B). Striking intensity correlations between the two beams are evident. The ratio between the observed Stokes and anti-Stokes fields was generally smaller than unity because of incomplete retrieval. We experimentally determined that the observed retrieval efficiency (10 to 30%) was limited by (in order of decreasing relevance) imperfect spatial

mode matching, power limitation of our retrieve beam laser, the ground-state coherence time, and possibly by the multilevel Zeeman structure of rubidium.

These observations can be viewed as resulting from a resonant four-wave frequency mixing process in a highly dispersive medium (21, 35). A high degree of intensity correlations is common for nonlinear parametric processes (as is well-known, e.g., for parametric down-conversion) (29, 32, 33, 36). However, the effect demonstrated here has one important distinction. In down-conversion, photon pairs are emitted simultaneously to an exceptionally high accuracy (30). Close examination of the data in Fig. 2C indicates that this is not true in the present case: The anti-Stokes fluctuations are delayed with respect to Stokes fluctuations. Experimentally, this delay could be varied in the range of 50 ns to about 1 μs; for example, increasing the intensity of the retrieve beam gave a shorter delay.

The delay in Fig. 2 corresponds to the finite time required for the retrieve beam to convert the atomic excitation into anti-Stokes light. To further illustrate this point, we theoretically analyzed the propagation dynamics of a fluctuation of the Stokes field in the presence of cw control beams (Fig. 2D). The delay originates from the time interval after the atomic spin flip (from $|g\rangle$ to $|s\rangle$) in which the anti-Stokes pulse components are still weaker than those of the Stokes light. During this interval, the group velocity of the Stokes field is close to the speed of light in vacuum c, whereas the group velocity v_g of the near-resonant anti-Stokes field is greatly reduced ($v_g \ll c$). After this initial retrieval stage, the two pulses lock together and propagate with equal group velocities, being simultaneously amplified further in a four-wave mixing process. Theoretical estimates from Fig. 2D for parameters corresponding to our experiment yield delays from 100 ns to 1 μs, comparable with the experimental observations.
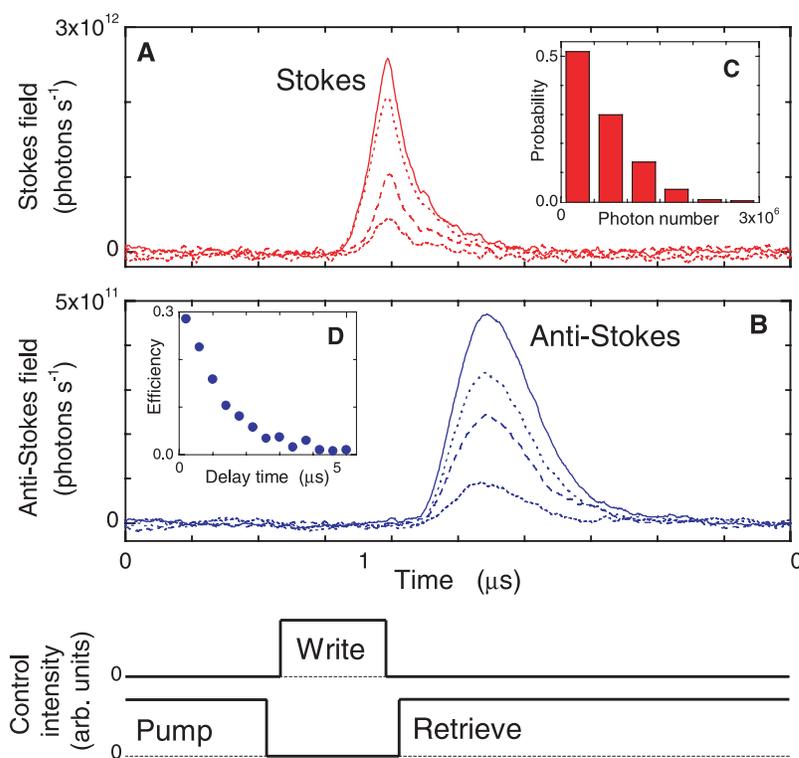
Fig. 3. Spontaneous Stokes signals (**A**) and retrieved anti-Stokes signals (**B**) from light storage with pulsed control beams. The retrieve control beam is first used for optical pumping, followed by nonoverlapping write and retrieve control pulses that create and retrieve Stokes and anti-Stokes signals. The traces below the data plot represent the modulation of the control beams. Consecutive realizations of the experiment with identical control parameters (solid, dotted, etc.) show strong fluctuations in the Stokes signal pulse energy and correlated fluctuations in the anti-Stokes pulse. Without the write control pulse or without the pump pulse, both the Stokes and anti-Stokes signals vanish. Removing the retrieve control pulse after the write control pulse showed results with only Stokes signals. (Weak background signals from control beams leaking through the filters are subtracted; the signal pulse shapes are limited by the detection bandwidth.) (**C**) Histogram of Stokes pulse energies. The distribution closely resembles a negative exponential as a function of pulse energy, confirming super-Poissonian photon number statistics of the spontaneous Stokes transition. (**D**) Retrieval efficiency (ratio of the average energy in anti-Stokes and Stokes pulses) as a function of the time delay between the end of the write control pulse and the onset of the retrieve control pulse. The exponential decay in retrieve efficiency agrees with the time scale for diffusive motion of atoms out of the control beam volume.

Thus, the observed delay corresponds to a temporal storage of the excitation in spin states.

The essential feature of the present technique is that the delay, and hence the storage time, can be controlled using time-varying write and retrieve control beams. Figure 3 shows the results of pulsed experiments in which a write pulse is followed by a retrieve pulse after a controlled time delay. We find again that, at fixed control pulse intensities and durations, the Stokes and anti-Stokes pulses strongly fluctuate from pulse to pulse in a highly correlated manner. The average amplitude of the anti-Stokes pulses decreases with increasing time delay as a result of atomic diffusion out of the control beam volume. We could observe retrieved pulses for up to 3 μs, and the fall-off in retrieve intensity is in good agreement with the atomic diffusion–limited coherence time for the present setup. Previous related experiments have been carried out for weak, coherent, classical pulses (*22, 23*); the present results demonstrate storage and retrieval of a spontaneously created hyperfine coherence.

We now turn to investigating the degree of correlations between the Stokes and anti-Stokes beams. To this end we obtained Raman signals with cw control beams, recorded signal intensities with high resolution, and analyzed the spectral densities of the Raman signal fluctuations by discrete Fourier transform. The fluctuation spectra of the Stokes and anti-Stokes fields are peaked at low frequencies, with the large noise reflecting the super-Poissonian nature of single-mode spontaneous Raman excitations (Fig. 4A). The spectral half-width of this spontaneous noise could be tuned in the range 100 kHz to 1 MHz (with tails up to about 2 MHz) by varying the write and retrieve beam intensities and the write beam detuning. At higher frequencies, the measured spectra generally approach a flat noise floor. Correlations between the two beams result in a large noise reduction in the spectrum of the signal that is formed by subtracting the Stokes and anti-Stokes signals in the time domain. In this difference intensity analysis, it was essential to compensate for the unbalanced intensities and the delay between the Stokes and anti-Stokes beams (*37*). We routinely observed 30 dB of intensity correlations over a broad range of low frequencies. The degree of subtraction is limited by the precision of the electronic components used in our detection system. Although this level of subtraction was not sufficient to eliminate spontaneous noise entirely at low frequencies, this was readily achieved in the higher frequency range where fluctuations in the Raman fields were smaller. Whereas at large frequencies the difference intensity noise approaches a flat noise floor, at intermediate values (near the high end of the Raman bandwidth) the difference intensity noise consistently drops a few percent below that level.

To quantify the degree of correlations in this intermediate regime, we performed several experimental tests. The benchmark level representing nonclassical effects is set by the photonic shot noise (PSN) associated with the Poissonian photon number statistics of coherent classical light (*38*), and it corresponds to a flat fluctuation spectrum. We performed several checks to define the PSN level. The difference signal for two output beams from a single laser beam on a beam splitter had a flat fluctuation spectrum at a level that was linearly (rather than quadratically) dependent on beam intensity, as is characteristic for PSN. The measured level of the fluctuation spectrum is in excellent agreement with PSN values calculated using the shot-noise formula and independently determined detector and amplifier parameters (taking into account an offset from the detector dark-noise levels; the data in Fig. 4 represent noise with contributions from both detected fields and detector dark noise). In addition to this PSN calibration, we performed a control experiment by measuring the difference signal between two beams formed by splitting the Stokes field on a beam splitter. In this measurement, the average intensity in each detection channel was carefully adjusted to match the Stokes and anti-Stokes channels in the correlation measurement of Fig. 4. This control experiment yielded a flat noise spectrum in agreement with the PSN level (gray line in inset, Fig. 4A) and, unlike the green line in Fig. 4, did not show the reduced noise level around 1.6 MHz. This confirms that the Stokes/anti-Stokes difference spectrum in Fig. 4A (green) drops at intermediate frequencies about 4% below the PSN level. Finally, Fig. 4B shows that the degree of correlations depends sensitively on the delay compensation between the Stokes and anti-Stokes signals: The onset of nonclassical correlations appears only when one properly compensates for the time that the atoms spend in a spin-flipped state. This sensitivity to delay compensation represents evidence for temporal storage of nonclassical states in atomic ensembles.

Several factors limit the degree of the observed quantum correlations. One of the most important limitations is associated with the incomplete retrieval process. The retrieval efficiency (10 to 30%) does not allow for large quantum correlations to be observed. In the present experiment, the retrieval efficiency was limited by imperfect spatial mode matching and the available laser power. We believe that a significant improvement in the efficiency can be realized using stronger laser fields with well-defined spatial modes. Finally, at lower light levels [as required for many applications (*6*)], the relative magnitude of the super-Poissonian noise is lower. This will in practice greatly extend the bandwidth of the nonclassical correlations. Our approach enables the generation and temporary storage of spin wave states in an atomic ensemble as well as retrieval of these
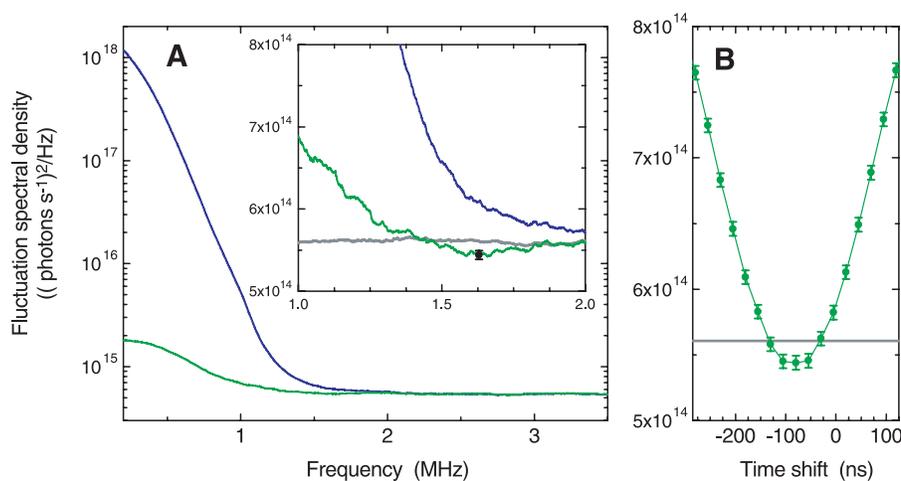
Fig. 4. Quantifying correlations between Stokes and anti-Stokes signals as in Fig. 2. (**A**) The fluctuation spectral density of the anti-Stokes field (blue) and of the signal formed by subtraction of the Stokes and anti-Stokes signals in the time domain [green (*37*)]. The spectrum of the Stokes fluctuations is not shown but is nominally identical to that of the anti-Stokes signal. The super-Poissonian character of the Raman signals leads to strong fluctuations at low frequencies (within the Raman bandwidth). At high frequencies (outside the Raman bandwidth), the fluctuation spectrum of the subtracted signal is flat and set by the shot-noise level for photon detection, and agrees with the independently determined level for the PSN. At frequencies near the high end of the Raman bandwidth (around 1.6 MHz; see the inset), the fluctuations in the subtracted signal fall bellow the measured PSN (gray curve in the inset). The observed onset of nonclassical correlations is limited by the finite retrieval efficiency and by the dark-noise levels of the detectors. The data point at 1.6 MHz shows an error bar of ±1 SD. The data are the result of averaging over 23 data sets, each of duration 2 ms and retrieval efficiency 10%, taken with identical control parameters over the course of 1 hour. The spectra have an averaging bandwidth of 200 kHz. (**B**) The fluctuation spectral density levels at 1.6 MHz (green) for the green line in (A), for different values of the time shift between Stokes and anti-Stokes signals before subtraction (*37*). The level at 1.6 MHz only drops below the measured PSN level (gray line) for time shifts around 81 ns, in agreement with the observed delay between the Stokes and anti-Stokes signals for this data set.

states by mapping onto correlated nonclassical states of light, raising the possibility of applications in quantum information science.

Note added in proof: We have been made aware of related work recently published by Kuzmich *et al.* (*39*).

References and Notes

1. D. Bouwmeester, A. Ekert, A. Zeilinger, Eds., *The Physics of Quantum Information* (Springer, Berlin, 2000).
2. H. J. Briegel, W. Dür, J. I. Cirac, P. Zoller, *Phys. Rev. Lett.* **81**, 5932 (1998).
3. J. I. Cirac, P. Zoller, H. J. Kimble, H. Mabuchi, *Phys. Rev. Lett.* **78**, 3221 (1997).
4. C. J. Hood, T. W. Lynn, A. C. Doherty, A. S. Parkins, H. J. Kimble, *Science* **287**, 1447 (2000).
5. P. W. H. Pinkse, T. Fischer, P. Maunz, G. Rempe, *Nature* **404**, 365 (2000).
6. L. M. Duan, M. D. Lukin, J. I. Cirac, P. Zoller, *Nature* **414**, 413 (2001).
7. A. Kuzmich, K. Molmer, E. S. Polzik, *Phys. Rev. Lett.* **79**, 4782 (1997).
8. M. D. Lukin, S. F. Yelin, M. Fleischhauer, *Phys. Rev. Lett.* **84**, 4232 (2000).
9. M. D. Lukin, *Rev. Mod. Phys.* **75**, 457 (2003).
10. S. E. Harris, *Phys. Today* **50**, 36 (July 1997).
11. K. J. Boller, A. Imamoglu, S. E. Harris, *Phys. Rev. Lett.* **66**, 2593 (1991).
12. M. O. Scully, M. S. Zubairy, *Quantum Optics* (Cambridge Univ. Press, Cambridge, 1997).
13. S. E. Harris, J. E. Field, A. Imamoglu, *Phys. Rev. Lett.* **64**, 1107 (1990).
14. M. D. Lukin, P. Hemmer, M. O. Scully, *Adv. At. Mol. Opt. Phys.* **42B**, 347 (1999).
15. L. V. Hau, S. E. Harris, Z. Dutton, C. H. Behroozi, *Nature* **397**, 594 (1999).
16. M. M. Kash *et al.*, *Phys. Rev. Lett.* **82**, 5229 (1999).
17. M. Fleischhauer, U. Rathe, M. O. Scully, *Phys. Rev. A* **46**, 5856 (1992).
18. K. M. Gheri, D. F. Walls, M. A. Marte, *Phys. Rev. A* **50**, 1871 (1994).
19. A. Imamoglu, H. Schmidt, G. Woods, M. Deutsch, *Phys. Rev. Lett.* **79**, 1467 (1997).
20. A. Imamoglu, H. Schmidt, G. Woods, M. Deutsch, *Phys. Rev. Lett.* **81**, 2836 (1998).
21. M. D. Lukin, A. B. Matsko, M. Fleischhauer, M. O. Scully, *Phys. Rev. Lett.* **82**, 1847 (1999).
22. C. Liu, Z. Dutton, C. H. Behroozi, L. V. Hau, *Nature* **409**, 490 (2001).
23. D. F. Phillips, A. Fleischhauer, A. Mair, R. L. Walsworth, M. D. Lukin, *Phys. Rev. Lett.* **86**, 783 (2001).
24. A. S. Zibrov *et al.*, *Phys. Rev. Lett.* **88**, 103601 (2002).
25. J. Hald, J. L. Sorensen, C. Schori, E. S. Polzik, *Phys. Rev. Lett.* **83**, 1319 (1999).
26. A. Kuzmich, L. Mandel, N. P. Bigelow, *Phys. Rev. Lett.* **85**, 1594 (2000).
27. B. Julsgaard, A. Kozhekin, E. S. Polzik, *Nature* **413**, 400 (2001).
28. M. G. Raymer, I. A. Walmsley, *Prog. Opt.* **28**, 181 (1996).
29. S. E. Harris, M. K. Oshman, R. L. Byer, *Phys. Rev. Lett.* **18**, 732 (1967).
30. C. K. Hong, Z. Y. Ou, L. Mandel, *Phys. Rev. Lett.* **59**, 2044 (1987).
31. M. Fleischhauer, M. D. Lukin, *Phys. Rev. Lett.* **84**, 5094 (2000).
32. O. Aytür, P. Kumar, *Phys. Rev. Lett.* **65**, 1551 (1990).
33. D. T. Smithey, M. Beck, M. Belsley, M. G. Raymer, *Phys. Rev. Lett.* **69**, 2650 (1992).
34. Experimental details are available as supporting material on *Science* Online.
35. P. R. Hemmer *et al.*, *Opt. Lett.* **20**, 982 (1995).
36. A. Heidmann, R. J. Horowicz, S. Reynaud, E. Giacobino, C. Fabre, *Phys. Rev. Lett.* **59**, 2555 (1987).
37. In the case where optical fields have losses before detection, the level of twin-mode squeezing that can be observed is reduced (*32*). For our data, the anti-Stokes signal appears identical to the Stokes signal, except for an apparent attenuation by a factor of ~5 and a time shift (Fig. 2C). In this case, twin-mode squeezing can still be investigated when the time shift is compensated and when the unbalanced attenuation is compensated by unbalanced linear amplification of the two signals. We

Superluminal and Slow Light Propagation in a Room-Temperature Solid

Matthew S. Bigelow,* Nick N. Lepeshkin, Robert W. Boyd

We have observed both superluminal and ultraslow light propagation in an alexandrite crystal at room temperature. Group velocities as slow as 91 meters per second to as fast as −800 meters per second were measured and attributed to the influence of coherent population oscillations involving chromium ions in either mirror or inversion sites within the crystal lattice. Namely, ions in mirror sites are inversely saturable and cause superluminal light propagation, whereas ions in inversion sites experience conventional saturable absorption and produce slow light. This technique for producing large group indices is considerably easier than the existing methods to implement and is therefore suitable for diverse applications.

Propagation of light pulses through material systems has been studied quantitatively for almost a century (*1*). It has been understood that the group velocity (v_g) of a pulse passing through a resonant system could be slower than the velocity of light in a vacuum (*c*) or could even be faster than *c* without contradicting the causality principle (*2–5*). Recently, techniques have been developed that have brought the control over the group velocity of light to such extremes as ultraslow light ($v_g \ll c$) (*6–9*), fast light ($v_g > c$ or v_g is negative) (*10–13*), and "stored" or "stopped" light (*14, 15*). These techniques hold promise for uncovering new physical phenomena and for practical applications such as controllable optical delay lines, optical data storage, optical memories, and devices for quantum information.

In the first experimental observation of slow and fast light propagation in a resonant

system (*16*), laser pulses propagated without appreciable shape distortion but experienced very strong resonant absorption ($\sim 10^5$ cm^{-1}). To reduce absorption, most of the recent work on slow light propagation has used electromagnetically induced transparency (EIT) to render the material medium highly transparent (*17, 18*) and still retain the strong dispersion required for the creation of slow light. Using this technique, a group velocity of $v_g = c/165$ in a 10-cm-long Pb vapor cell was observed (*6*). More recently, a group velocity of 17 m/s was found for propagation in a Bose-Einstein condensate (*7*), and a modulation technique was used to measure a group velocity of 90 m/s in Rb vapor (*8*). Using similar techniques, group velocities as low as 8 m/s have been inferred (*9*). Solid-state materials have also been used to observe the propagation of slow light with a velocity of 45 m/s through Pr-doped Y_2SiO_5, maintained at a cryogenic temperature of 5 K (*19*).

There also has been considerable work in the production of fast light. Electromagnetically induced absorption has been used

---
The Institute of Optics, University of Rochester, Rochester, NY 14627, USA.

*To whom correspondence should be addressed. E-mail: mbigs@optics.rochester.edu